# Ultrafast Energy Transfer Dynamics in a Cyanobacterial Light-Harvesting Phycobilisome

Chao Xiao , Na Guo , Zidong Liang , Zhencheng Huang , Wenjun Li , Mingyuan Xie * , Fuli Zhao *

Posted Date: 26 April 2023

doi: 10.20944/preprints202304.0938.v1

Keywords: light-harvesting antenna; phycobilisomes; time-resolved spectroscopy; energy transfer

*Article*

# Ultrafast Energy Transfer Dynamics in a Cyanobacterial Light-Harvesting Phycobilisome

**Chao Xiao [1], Na Guo [1], Zidong Liang [1], Zhencheng Huang [1], Wenjun Li [2,3], Mingyuan Xie [1,*] and Fuli Zhao [1,*]**

[1] School of physics, State Key Laboratory of Optoelectronic Materials and Technologies, Sun Yat-sen University, Guangzhou, 510275, China; xiaoch23@mail2.sysu.edu.cn; (C.X.), guon28@mail2.sysu.edu.cn; (N.G.), liangzd@mail2.sysu.edu.cn; (Z.L.), hzhench2@mail.sysu.edu.cn; (Z.H.)

[2] Yantai Institute of Coastal Zone Research, Chinese Academy of Sciences, Yantai, 264003, China; wjli@yic.ac.cn; (W.L.)

[3] Center for Ocean Mega-Science, Chinese Academy of Sciences, Qingdao 266071, China

* Correspondence: xiemy5@mail.sysu.edu.cn; (M.X.), stszfl@mail.sysu.edu.cn; (F.Z.)

**Abstract:** The phycobilisomes (PBS) of cyanobacteria and red algae are the primary light-harvesting antennas, absorbing solar energy and transporting it to photosynthetic reaction centres with extraordinary efficiency and rate. The mechanism of energy transfer in PBS should be investigated in conjunction with biological structural information, as the functions of proteins result from structures. Here, we report the energy transfer study in PBS from a thermophilic cyanobacterium *Thermosynechococcus vulcanus NIES 2134* (*T. 2134*), with the Cryo-EM model resolved at near-atomic-resolution recently. The time-resolved fluorescence spectroscopy of PBS with the sub-picosecond resolution was discovered at 77K. Deconvolution of the fluorescence decay curve was then used to reveal the energy transfer channels and the associated transfer rates. Expert for the fluorescence lifetimes of terminal emitters, four time-components, i.e., 9 ps, 13 ps, 23 ps, and 55 ps, were recognised in the energy transfer in PBS. The energy transfer dynamics in PBS were further analysed by combining the cryo-EM structure and the spectral property. The findings aid our understanding of the energy transfer mechanisms in PBS.

**Keywords:** light-harvesting antenna; phycobilisomes; time-resolved spectroscopy; energy transfer

## 1. Introduction

Cyanobacteria, or Cyanophyta, are aquatic gram-negative bacteria [1]. It is widely accepted that cyanobacteria are the first organisms known to have created oxygen via photosynthesis. In addition, by creating and evolving the molecular oxygen as a byproduct of photosynthesis, the live and multiply of cyanobacteria has changed the early oxygen-poor and allowed for the emergence of diverse life forms on earth [2]. Unlike purple and other bacteria that perform anoxygenic photosynthesis, cyanobacterial thylakoid membranes are not continuous with the plasma membrane but have separate compartments [3]. These thylakoid membranes have an important function in photosynthesis, as they host PBS which functions as a primary light-harvesting antenna for the photosystems [4]. Those PBS are composed of chromophorylated protein stacks, referred to as phycobiliproteins (PBPs) and linker proteins. The PBS assumes a classical structure, wherein the allophycocyanin (APC) performs the core of the model, surrounded by several outwardly oriented rods made up of stacked disks of phycocyanin (PC) and phycoerythrin (PE). In an antenna-like assembly, the geometrical arrangement of the PBPs is exquisite. This intricate arrangement facilitates high efficacy in the transmission of excitation of PBS [5].

To provide an enhanced understanding of the energy transfer process in PBS, scientists have explored the protein's energy distribution and energy transfer model through steady-state and transient spectra, concerning the unique spectral property of different PBPs [6,7]. PBPs' spectral

Preprints (www.preprints.org) | NOT PEER-REVIEWED | Posted: 26 April 2023 doi:10.20944/preprints202304.0938.v1



properties are primarily determined by their prosthetic groups, which are linear tetrapyrroles known as phycobilin, including phycocyanobilin (PCB), phycoerythrobilin (PEB), and phycourobilin (PUB) [8]. Each PBP has a distinct maximum absorption and fluorescence emission in the visible range of light. As a result of their presence and the specific arrangement within the PBS, light energy can be absorbed and transferred uni-directionally to the chlorophyll of photosystem II. In this way, the PBPs take advantage of available light wavelengths (in the 500-650 nm range) that chlorophyll cannot access and use their energy for photosynthesis [9,10]. This is especially beneficial deeper in the water column, where longer wavelength light is less transmitted and thus less available directly to chlorophyll. The light-trapping function of phycobilisome and phycobilin arises from variations in protein arrangement and microenvironment of prosthetic groups. Sole reliance on phycobilin spectral results falls short in explaining the intricate energy transfer process, which must be understood through a synergistic approach combining spectral properties, protein structure, and composition to derive functional insights from structural features. It is much to be regretted that only five detailed architectures of PBS have been described by cryo-electron microscopy (cryo-EM) with great resolution at the near-atom level: two red alga species *Griffithsia pacifica* [11], *Porphyridium purpureum* [12], three cyanobacterial species, *Anabaena 7120*, *Synechococcus 7002* [13] and *Thermosynechococcus vulcanus 2134* [14]. Therefore, it is challenging to interpret the complex energy transfer process and mechanism in phycobilisomes.

As mentioned above, the energy transfer dynamics of thermophilic cyanobacterium *T.2134* are controversial in the absence of a high-resolution protein structure. In 2003, Adir et al. discovered a minor fraction of PC that absorbed maximally at 612 nm during the isolation of APC from *T. 2134* [15]. This unique $PC_{612}$ trimmer was thought to cover the space between the lower base core cylinders and the higher cylinder in the APC core at the ends of two of the rods. Based on this structural model, they discovered a quick energy transfer pathway that took 888 fs to go from the rod to the core via linker proteins, and then 17 ps to get from the core to the terminal emitters ($L_{CM}$) [16]. Then, using ps fluorescence and fs pump-probe spectroscopies, Kawakami et al. discovered the energy transfer of 7.3 ps between PC trimers in rods, 53 ps from PC rod to APC core, and 180 ps in the APC core complex [17]. They also confirmed that the APC trimer, not the $PC_{612}$ trimer, is located between the lower base core A cylinders and the higher B cylinder [18]. Until recently, the APC core and PC rod of *T. 2134* were resolved at 3.7 and 4.2 resolutions, respectively, yielding the results that the PBS molecule of *T. 2134* consists of 5 APC core cylinders (A, A′, B, C, C′) surrounded by 8 PC rods (Rb, Rb', Rt, Rt', Rs1, Rs1', Rs2, Rs2'), as shown in Figure 1, which provide the structural basis for energy transfer research. Hence, with a focus on the PBS rod-core assembly [19], we aim to re-identified the energy transfer path of the thermophilic cyanobacterium *T. 2134* via fs time-resolved fluorescence spectra and high-resolution structures.

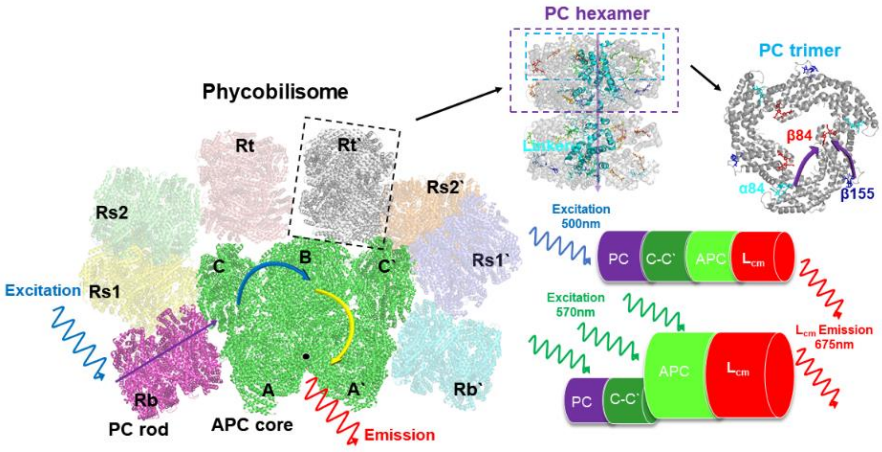


**Figure 1.** Architecture diagram of the PBS from *T. 2134*. This overall PBS model was drawn referencing the PBS structures from *Anabaena and Thermosynechococcus vulcanus* [13,14].

Preprints (www.preprints.org) | NOT PEER-REVIEWED | Posted: 26 April 2023 doi:10.20944/preprints202304.0938.v1



## 2. Materials and Methods

### *2.1. Growth of cyanobacteria and isolation of PBS*

*T. 2134* was grown in BG11 medium at 39°C, under light illumination (light cycle 16 h, dark cycle 8 h), with the air supply through 0.22 μm filters.

After 7 days of culture, PBS was isolated from *T. 2134*, based on the methods of Professor Gantt's extraction, with some minor changes [20]. Briefly, the PBS was extracted at 18 °C with pH 7.0, 0.75 mol/L $Na_2HPO_4$-$KH_2PO_4$ phosphate buffer containing 0.5 mol/L sucrose and 10 mmol/L EDTA as a buffer system. (1) The algal cells were harvested through centrifugation at 6000g for 10 min and then rinsed twice in pH 7.0 phosphate buffer to collect the precipitate. (2) After 3g wet weight was collected to the total volume of 10 ml with phosphate buffer following a final concentration of 1 mmol/L PMSF (protease inhibitor), and then the cells were disrupted by French press (4000psi, twice) [21]. (3) Add to a final concentration of 2% Triton X-100 to dissolve the thylakoid membrane, and add to a final concentration of 1 mmol/L PMSF again. Occasionally very gentle shaking per 2 min for 30~40 min in the dark. (4) The above solution was treated by ultracentrifugation (Centrifuge with a Beckman Coulter Optima XPN-100 ultracentrifuge, SW41Ti rotor, centrifugal force RCF av= 20,000 g (12150 rpm) at 18 °C for 45 min). (5) The resulting supernatant from the above ultracentrifugation was placed in gradient sucrose solution (0.5, 0.75, 1.0, 1.5, 2.0 mol/L sucrose in 0.75mol/L phosphate buffer), then were ultracentrifuged using SW41Ti rotor, with centrifugal force RCF av= 120,000 g (37400 rpm) at 18 °C for 4 h. The target PBS was collected from a 1 mol/L sucrose layer.

### *2.2. Determination of time-resolved spectral properties*

Figure 2 shows the experimental setup for measuring time-resolved spectra. At a central wavelength of 800 nm, the experiment was carried out using a regenerative Ti: Sapphire amplifier system (Astrella, Coherent). After that, the excitation laser was tuned to 498nm and 570nm using a femtosecond OPA (OPerA Solo, Coherent) with a pulse duration of 35 fs and a repetition rate of 1 kHz. The output femtosecond laser beam was focused into a silica sample-holding cuvette, which was frozen in the dark after being submerged in liquid nitrogen, after passing through an aperture and a continuous attenuator. The fluorescence single of the sample was then collected by a synchroscan streak camera (C4742, Hamamatsu, time-resolution 700 fs) coupled to a polychromator, allowing for the detection of temporal characteristics. The time resolution of the time-resolved fluorescent spectrum measurement is primarily determined by the response time of the streak camera and the width of the stimulation pulse. The streak camera's response time is less than 1 ps, and accounting for the dispersion effect of optical elements and time jitter of the synchronous trigger signal, the overall system time resolution is under 2 ps. All the measurements were carried out at a temperature of 77K.

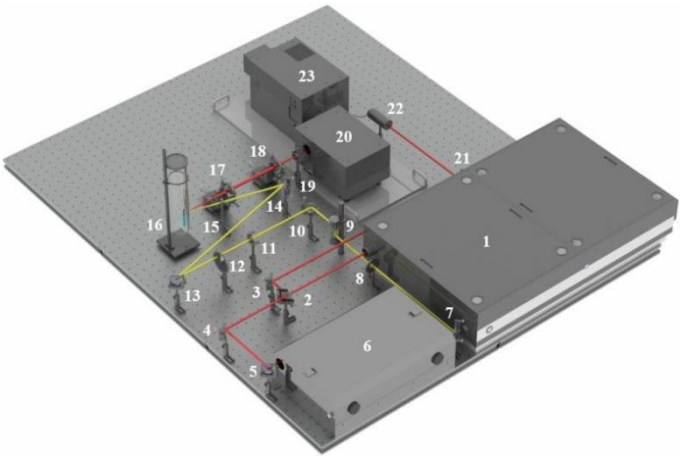


**Figure 2.** Experimental setup for time-resolved spectra measurement. 1: Ti: Sapphire Amplifier; 2: Beam splitter; 3,4,5,7,10,13,14,21: Mirror; 6: OPA; 8: Aperture; 9: Beam lifter; 11: Neutral filter; 12:

Attenuator; 15,17,18: Lens; 16: Cryostat & Cuvette; 19: High-pass filter; 20: Streak Camera; 22: Synchronous trigger; 23: Polychromator.

*2.3. Time-resolved fluorescence spectra analysis*

The two-dimensional fluorescence lifetime image acquired by the streak camera encodes the lifetime and wavelength characteristics of the fluorescent molecule on the horizontal and vertical axes, respectively. In the wavelength direction, the fluorescence decay kinetic curve can be obtained by cutting the image at the appropriate spacing and summing the number of photons accumulated in the cutting region. After assuming different exponential decay components, the dataset containing the fluorescence decay curve can be further analyzed by using the multi-exponential fitting method. To avoid additional statistical errors caused by different measurement results in the fitted results, and ensure the strict consistency of the laws obtained in different measurements, the global optimization method is used [22]. In addition, the global optimization method assumes that the time and wavelength characteristics of fluorescence molecules are separable, which means that the contribution of the lifetime of individual fluorescence decay component to the overall fluorescence decay is independent of the emission wavelength, i.e., the spectrum of species or states is constant. Therefore, for the entire dataset, the fluorescence decay curves for different bands can be fitted simultaneously with the same parameters, and only amplitude variations are allowed between emission wavelengths. By using lifetime parameters as a global fitting parameter, multiple groups of experimental data are fitted, and we obtain the fluorescence decay-associated spectra (FDAS) corresponding to the wavelength. FDAS was provided by the amplitudes of these exponential components as a function of emission wavelength [23]. During data processing, it is necessary to deconvolve the fluorescence images acquired by the streak camera [24,25]. Here, $F_{exp}$ represents the detected fluorescence intensity, which is described as follows:

$$F_{exp}(t) = f_{pump} \otimes F_{theo} = \int f_{pump}(t) F_{theo}(t - t') dt' \quad (1)$$

Where $f_{pump}$ is the time response function of the test instrument to the pulse. In this case, we considered the theoretical fluorescence intensity $F_{theo}$ as a multi-exponential sum:

$$F_{theo}(t) = \sum \varepsilon_i \exp(-t/\tau_i) \quad (2)$$

To fit the isotropic fluorescence, we used a deconvolution procedure based on a global optimization algorithm described below [23]. The amplitude of the fluorescence isotropic decay constant of $\tau_i$ is denoted by A.

$$I_n(\lambda, t) = \sum_{i=1}^{n} A_i(\lambda_i) \exp(-t/\tau_i) \quad (3)$$

## 3. Results and Discussion

The steady-state absorption spectra of the isolated PC trimer and APC core from *T.2134*, as well as the entire PBS, have been resolved at room temperature [19]. The absorption band of the intact PBS peaked at 620 nm. The absorption band of the isolated PC rod also peaked at 620nm but exhibited narrower than that of the intact PBS, whereas, the absorption band of the APC core performed as a broadening on the red side of the PC trimer, peaking at 650 nm with a shoulder at 600 nm. The PC rod then exhibited a fluorescence peak at 650 nm, while the peak of the APC fluorescence was around 675 nm. We further measured the spectra property of the C-cylinder of the core, with the absorption band peaked at 612nm and the emission band peaked at 645nm [26]. In steady state, the emissions from various fluorescence components combine to form the fluorescence spectra, therefore, to investigate the overall energy transfer dynamics in PBS, the time-resolved fluorescence spectra were performed, and the femtosecond laser at the wavelength of 498 nm and 570 nm was selected to excite the PBS sample, respectively. The steady-state absorption spectrum measurements show that only the PC trimer was excited under the wavelength of 500nm as the APC core has no absorption at the

Preprints (www.preprints.org) | NOT PEER-REVIEWED | Posted: 26 April 2023 doi:10.20944/preprints202304.0938.v1



wavelength of 498 nm [19,27], however, both the PC trimer and APC core can be exited under the wavelength of 570 nm.

The time-resolved fluorescence spectra of *T.2134* PBS at 77 K were thoroughly examined. High signal-to-noise ratios are made possible by the ability to ignore solvent and molecule vibration effects at 77 K, which ensures that the results of time-resolved fluorescence spectroscopy closely match the energy transfer assumptions required in theoretical models [28]. Figure 3a exhibits the reconstructed three-dimensional time-resolved fluorescence spectra of PBS from *T. 2134* excited at 498nm. The expression aids us in conceptualizing the energy flow. Following excitation at 498 nm, which preferentially excited the PCBs of β155 in PC rods [27], the time-resolved fluorescence spectra of PBS revealed the PC fluorescence band with a central wavelength of around 655 nm, followed immediately by the fluorescence band of the C-cylinder at 645 nm, and the fluorescence band of the APC core at around 675 nm rose concurrently with the decay of C-cylinder. The immediate evidence of the energy transfer from PC→C-cylinder→APC is the changes in the relative intensities of fluorescence components. Different from the results of the 498 nm excitation time-resolved fluorescence spectra, the PC rod and APC core were exited simultaneously under the excitation wavelength of 570 nm. The time-resolved fluorescence spectra result shows that the PC and APC emissions were both discovered at the same time, as shown in Figure 3b.

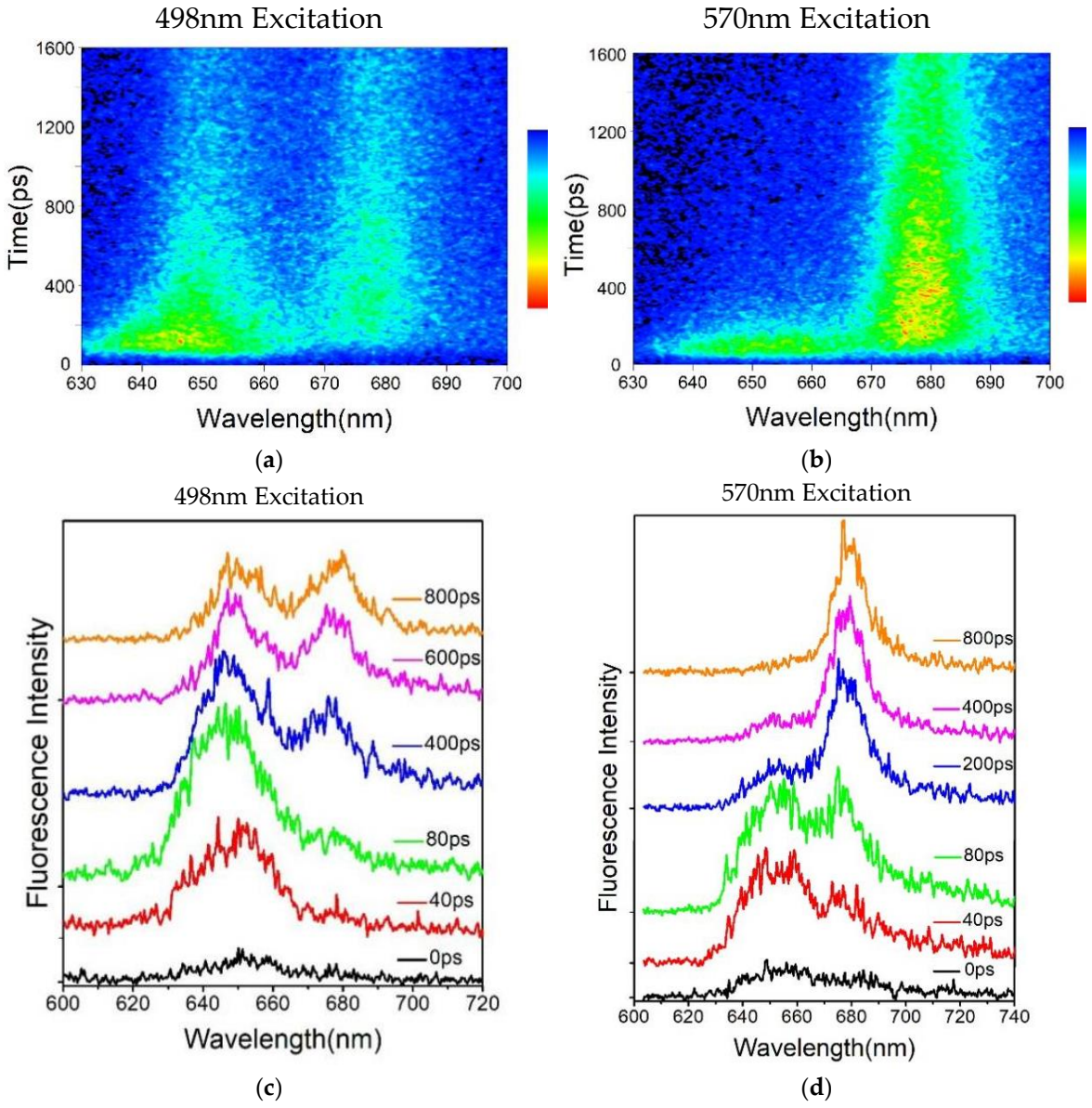

Preprints (www.preprints.org) | NOT PEER-REVIEWED | Posted: 26 April 2023 doi:10.20944/preprints202304.0938.v1



**Figure 3. (a)** Time-resolved fluorescence spectra of *T. 2134* PBSs at 77K, with the excitation wavelength set to 498 nm. **(b)** Time-resolved fluorescence spectra of *T. 2134* PBSs at 77K, with the excitation wavelength set to 570 nm. The fluorescence intensity is depicted as a gradient, with blue denoting low intensity and red denoting high intensity. (**c**) Time-resolved fluorescence spectra of *T. 2134* PBSs detected at different times after stimulation, with the excitation wavelength set to 498 nm. (**d**) Time-resolved fluorescence spectra of *T. 2134* PBSs detected at different times after stimulation, with the excitation wavelength set to 570 nm. The picoseconds after stimulation are shown by the numbers.

The variations in the fluorescence spectrum were seen to be more obvious in Figure 3c. Time-resolved fluorescence was discovered using synchronscan technology, and the 650 nm emission was initially clearly identified. And the APC emission appears at 40 ps after excitation, indicating that the terminal emitter in the core accepts the energy transferred from the PC rod within 40 ps. However, the PC emission quickly decayed and nearly disappeared at 400 ps after the excitation (Figure 3d), indicating that the energy transfer process between PC and APC was completed within 400 ps.

Global optimization deconvolution was used to find out the fluorescence decay constants in the PBS during energy transferring. Multi-exponential deconvolution was used to resolve the fluorescence decay curves at various measured wavelengths, and the Monte-Carlo approach was used to analyze the experimental data. An energy acceptor is represented by the component (A%) with a negative amplitude of the fluorescence's rising phase, while an energy donor is represented by the component (A%) with a positive pre-exponential of the fluorescence's falling phase.

Based on the results of the global multiexponential analysis, Figures 4c-d show the fluorescence decay-associated spectra (FDAS) obtained by the phycobilisome of *T.2134* under excitation at 498nm and 570nm, respectively. In combination with the high-resolution model, FDAS can further help to reveal the energy transfer in PBS. Typically, to explore the decay kinetics of the same decay constant in different wavelength regions, it is necessary to consider the kinetic increase and reduction of the excited component, that is the change of the amplitude of the kinetic phase. Moreover, the sign of the FDAS factor with the same decay constant is inverted, indicating that there is a coupling occurring between the positive and negative bands, i.e., that there is energy transferred from the complex of the former band that gives energy to the latter band.

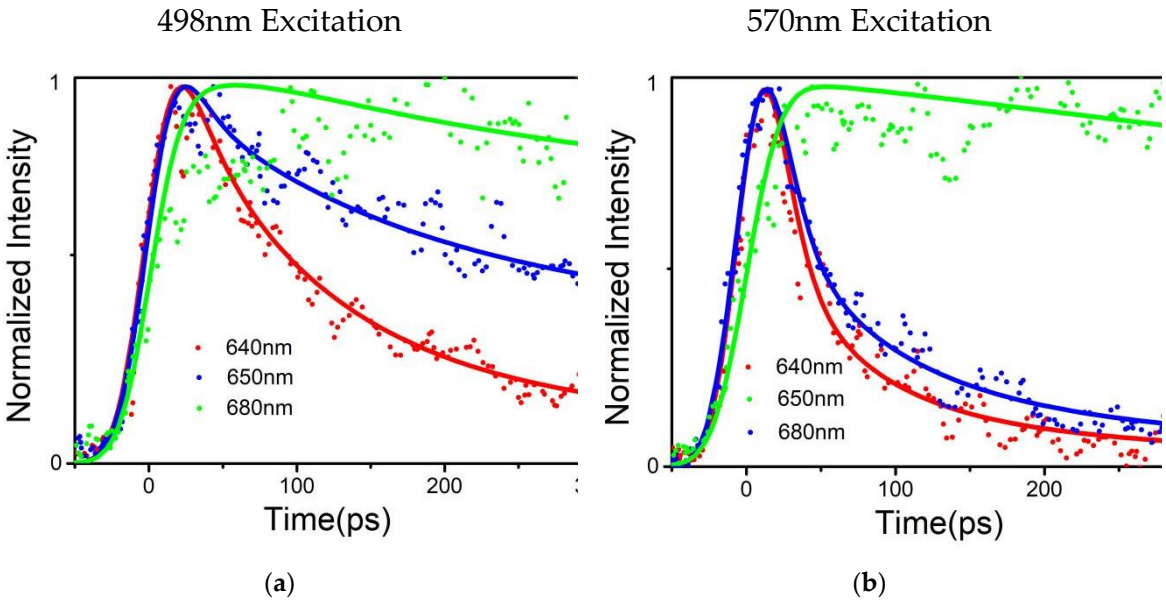


(**a**) (**b**)

Preprints (www.preprints.org) | NOT PEER-REVIEWED | Posted: 26 April 2023 doi:10.20944/preprints202304.0938.v1



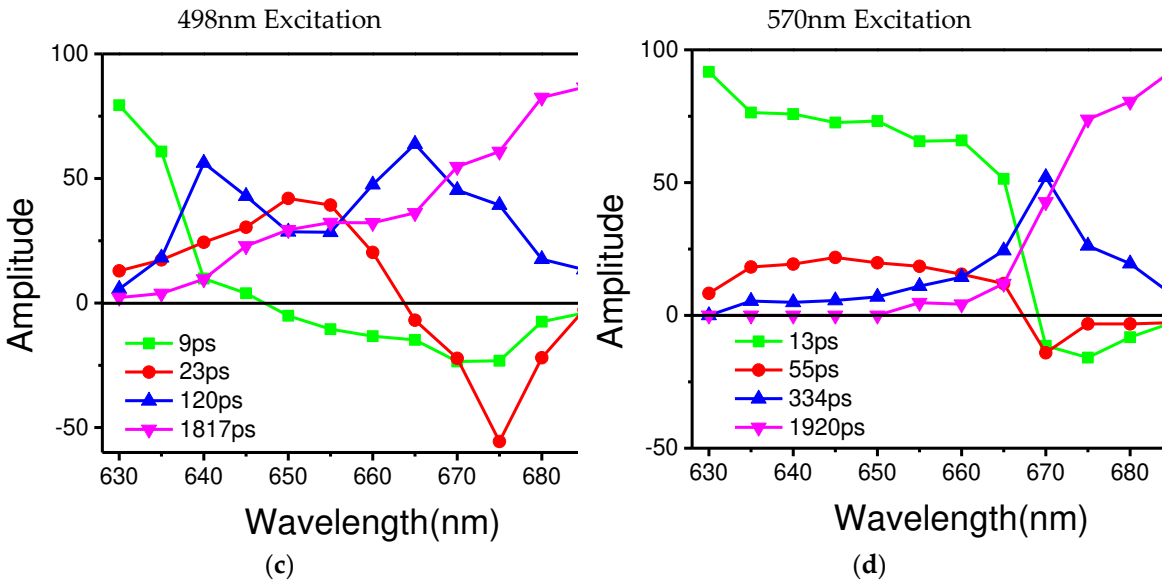


**Figure 4. (a)** Normalized fluorescence intensity decay curves of *T. 2134* PBSs, with the excitation wavelength set to 498 nm; **(b)** Normalized fluorescence intensity decay curves of *T. 2134* PBSs, with the excitation wavelength set to 570nm. Detection was done at 640 nm, 650 nm, and 680 nm, respectively. Dots represent the experiment data, and the lines represent the fitting results; **(c)** FDAS of *T. 2134* PBSs, with the excitation wavelength set to 498 nm; **(d)** FDAS of P. purpureum PBSs, with the excitation wavelength set to 570 nm.

From the results, the two excitation wavelengths produce two different sets of decay constants, 10 ps, 20 ps, 120 ps, and 1817 ps for 498 nm excitation, and 13 ps, 55 ps, 344 ps and 1920 ps for 570 nm excitation. In the support material, the fluorescence decay curves and the correspondent fitting results of PBS at different wavelengths are depicted in Figures S1 and S2, and Tables S1 and S2 show the amplitudes of each time component. Among these results, the four rapidly decaying DAS components, 9 ps, 13 ps, 23 ps and 55 ps, exhibit sign change from positive to negative, which are indicative of the decay of one fluorescence band in parallel with the rise of another, showing the characteristics of EET. The other four components had positive peaks without sign changes, indicating that their decay only occurred during the trapping or relaxation. In addition, considering the position of the sign shift and the peak in the horizontal direction, the four decay constants are clearly distinguished. The sign change of 9 ps appeared between 645 nm and 650 nm, while the sign change of 13 ps occurs between 665 nm and 670nm; similarly, the sign change of 23 ps occurs between 660 nm and 665 nm, 55 ps between 665 nm and 670 nm. The positive peaks occur at decay constants of 120 ps and 334 ps, while the decay constants of 1817 ps and 1920 ps gradually increase with increasing wavelength. Therefore, combined with the steady-state spectra and structural information, the FDAS results allow us to assign the following decay constants:

The 9 ps and 13 ps correspond to the fastest decay constants in Figures 4c-d, respectively. The 9 ps were constant of fluorescence decay in *T. 2134* PBS could be assigned to the time of energy transfer from the C/C′-cylinders direct to the terminal emitter ApcF/F′ in A/A′ cylinders of the APC core, owing to the fact that its amplitude began positively on the blue side before swiftly turning negative and having a minimum at 670 nm (as shown in Figure 4c). The negative amplitude corresponds to a fluorescence increase and energy transfer from donor to acceptor. Moreover, the latest APC Cryo-EM structure shows that there are strongly coupled pigment pairs between the C/C′ cylinders and the A/A′ cylinders, ${}^{C}\alpha^{84}$–${}^{A}\alpha^{84}$. The transferring of energy from the C/C′ cylinders to A/A′ cylinders occurring via ${}^{C}\alpha^{84}$–${}^{A}\alpha^{84}$ (35 Å), results in a fast energy transfer time of 9 ps [14]. Therefore, the quick transfer of energy between C/C'-cylinders and terminal emitter ApcF/F' can be assigned a decay time of 9 ps. The 13 ps constant of the fluorescence decay curve of *T. 2134* PBSs could be attributed to the process of energy transfer from the rod Rb/Rb′ and the C/C′ cylinders to the terminal emitter ApcE/E′ in A/A′ cylinders with the same transfer constant, Shown in Figure 4d, from 630 to 660 nm, its

 doi:10.20944/preprints202304.0938.v1



amplitude was positive. It then started to decline at 665 nm, turned negative at 670 nm, and finally reached a minimum at 675 nm. The following is a description of this amplitude variation: an acceptor with an emission peak of 675 nm receives energy from a donor with an emission peak between 630 and 660 nm. The light absorbed by PCBs in the rod Rb/Rb' was transferred directly to the ApcE/E' in A/A' cylinders via rod-core linker $L_{RC}$. At the same time, the light absorbed by PCBs in C/C' cylinders was transferred to the terminal emitter ApcE/E' in A/A' cylinders via core linker $L_C$. Thus, combining the fluorescence spectra and the cryo-EM structure of the APC core, it is reasonable to assign the decay time of 13 ps to the energy transfer time from the rod or the C/C' cylinders or B cylinder to the terminal emitter ApcE/E' in A/A' cylinders with same transfer constant.

For the decay constants of 23 ps and 55 ps, the experimental results at different excitation wavelengths can clearly see that the terminal receives the energy flow transferred from the PC rod or C/C' cylinders after 40 ps. Therefore, the 23 ps constant of fluorescence decay in *T. 2134* PBS could be assigned to the energy transfer time from the PC rod Rs/Rs' → C/C' cylinders →terminal emitter ApcE/E' in A/A' cylinders because at the blue side, the amplitude of the FDAS is positive with a maximum wavelength of around 650 nm, while at the red side, the amplitude shifts to the negative with a minimum at about 675 nm (Figure 4c). Compared with the constants of 9 ps, the higher amplitude of the FDAS curve of the constant of 23 ps shows that the energy transfer pathway with an energy transfer time of 23 ps takes to dominate in the energy transfer from the rods to the core. This agrees with the cryo-EM findings, which show that the C/C' cylinder serves as a conduit for energy transfer from the PC rods to the terminal emitters. Therefore, combining the fluorescence spectra and the cryo-EM structure of the PC rods and APC core, it is appropriate to provide the energy transfer time between Rs/Rs' rods and terminal emitter ApcE/E', a decay time of 23 ps. The 55 ps constant of fluorescence decay curve in *T. 2134* PBS could be attributed to the process of energy transfer time from the PC rod Rs/Rs'→the C/C' cylinders→the B cylinder→ the terminal emitter ApcD/D' in A/A' cylinders, which is a long energy transfer pathway from the rod to the terminal emitter. Because on the blue side, the amplitude of the FDAS is positive, having a maximum of 645 nm, while on the red side, the amplitude shifts to the negative with a minimum of about 670 nm. Moreover, the amplitude of 55 ps is low compared with that of 13 ps, indicating this energy transfer pathway is not the main pathway of the energy transfer from the rod to the core. Therefore, combining the fluorescence spectra and the cryo-EM structure of the PC rods and APC core, it is appropriate to give a decay time of 55 ps to the energy transfer from the PC rod Rs/Rs'→the C/C' cylinder→the B cylinder→the terminal emitter ApcD/D' in A/A' cylinders.

For the four decay constants without EET, the possible energy transfer paths are assigned according to their peak and the trend of the FDAS factor. The fluorescence isotropic decay constants of 1920 ps and 1817 ps reflect the emission of the terminal emitter ApcE (ApcE'). The 120 ps constant of fluorescence decay possibly reflects the emission of the rods and the C/C' cylinders, because a positive band with two peaks at 640 nm and 665nm was resolved in the FDAS. Due to the fact that only a positive band with a maximum at 670 nm was determined, the fluorescence decay constants of 334 ps may represent the emission of the APC core. The energy transfer dynamics of the intact PBS obtained in this study is summarized in Figure 5.

Preprints (www.preprints.org) | NOT PEER-REVIEWED | Posted: 26 April 2023 doi:10.20944/preprints202304.0938.v1



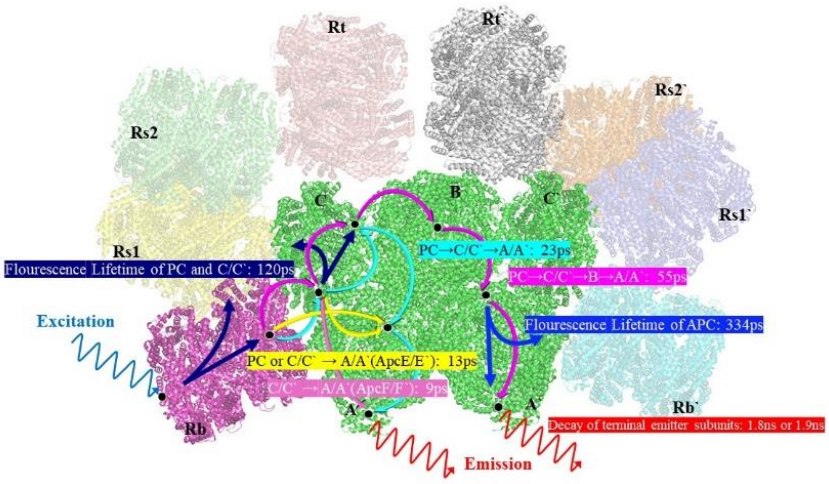


**Figure 5.** A schematic excitation energy transfer model of the PBS from *T. 2134.*

## 4. Conclusions

We investigated the dynamic process of energy transfer in the PBS from cyanobacteria by using femtosecond FRTS and the deconvolution method, giving the energy transfer pathways and the energy transfer time constants. The energy transfer dynamics were analyzed via simultaneous or sequentially exciting the rod and core, respectively. The results show that energy is transferred from PC rods to the terminal emitter through the C-cylinder as an intermediary, with a fast energy transfer rate of less the 10 ps interacting with the A-cylinder. The results of energy transfer dynamics from time-resolved PBS spectroscopy combined with biological structural information at high resolution provide insight into the energy transfer mechanism in PBS. More in-depth investigation dependent on the separation between chromophores and how they are arranged will illuminate the energy transfer dynamics more delicately.

**Author Contributions:** Supervised the project, M.X. and W.L.; prepared the samples, W.L. and C.X., steady-state microscopy data collection and analysis, W.L.; time-resolved spectroscopy measurement, C.X. and N.G.; the spectroscopy results analysis, Z.L. and Z.H.; writing—original draft preparation, M.X. and C.X.; writing—review and editing, F.Z. and W.L.; funding acquisition, M.X. All authors have read and agreed to the published version of the manuscript.

**Funding:** This research was funded by the National Key Research and Development Program of China, grant number 2021YFC2103900 and the Guangdong Provincial Scientific and Technological Program, grant number 2016B090918099 and the Open Fund of the State Key Laboratory of High Field Laser Physics (Shanghai Institute of Optics and Fine Mechanics).

**Data Availability Statement:** Experimental data are available upon reasonable request to the authors.

**Acknowledgments:** We thank the staff at the School of physics, State Key Laboratory of Optoelectronic Materials and Technologies, Sun Yat-sen University for technical support on the femtosecond laser system and streak camera performances.

**Conflicts of Interest:** The authors declare no conflict of interest.

## References

1. Sinha, R.P.; Häder, D.P. UV-protectants in cyanobacteria. *Plant Sci.* **2008**, 174(3), 278–89.
2. Schopf, J.W. The fossil record of cyanobacteria. In *Ecology of Cyanobacteria II: Their Diversity in Space and Time.* 1st ed.; Whitton, B.A. Eds.; Springer Science & Business Media: Berlin/Heidelberg, Germany, **2012**; Volume 63, pp. 15-36.
3. Vothknecht, U.C.; Westhoff. P. Biogenesis and origin of thylakoid membranes. *Biochim. Biophys. Acta - Mol. Cell Res.* **2001**, 1541, 91–101.
4. Croce, R.; van Amerongen, H. Natural strategies for photosynthetic light harvesting. *Nat. Chem. Biol.* **2014**, 10, 492–501.
5. Glazer, A.N. Light harvesting by phycobilisomes. *Annu. Rev. Biophys. Biophys. Chem.* **1985**, 14, 47–77.

6. Duysens, L. Transfer of light energy within the pigment systems present in photosynthesizing cells. *Nature* **1951**, 168, 548–550.
7. Xie, M.; Li, W.; Lin, H.; Wang, X.; Dong, J.; Qin, S.; Zhao, F. Diference in light use strategy in red alga between Grifthsia pacifca and Porphyridium purpureum. *Sci. Rep.* **2021**, 11, 14367.
8. Watanabe, M.; Ikeuchi, M. Phycobilisome: architecture of a light-harvesting supercomplex. *Photosynth. Res.* **2013**, 116, 265-276.
9. Saer, R.G.; Blankenship, R.E. Light harvesting in phototrophic bacteria: structure and function. *The Biochem. J.* **2017**, 474, 2107-2131.
10. Mullineaux, C.W. Phycobilisome-reaction centre interaction in cyanobacteria. *Photosynth. Res.* **2008**, 95, 175-182.
11. Zhang, J.; Ma, J.; Liu, D.; Qin, S.; Sun, S.; Zhao, J.; Sui, S. Structure of phycobilisome from the red alga Grifthsia pacifca. *Nature* **2017**, 551, 57–63.
12. Ma, J.; You, X.; Sun, S.; Wang, X.; Qin, S.; Sui, S. Structural basis of energy transfer in Porphyridium purpureum phycobilisome. *Nature* **2020**, 579, 146–151.
13. Zheng, L.; Zheng, Z.; Li, X.; Wang, G.; Zhang, K.; Wei, P.; Zhao, J.; Gao, N. Structural insight into the mechanism of energy transfer in cyanobacterial phycobilisomes. *Nat. Commun.* **2021**, 12, 5497.
14. Kawakami, K.; Hamaguchi, T.; Hirose, Y.; Kosumi, D.; Miyata, M.; Kamiya, N.; Yonekura, K. Core and rod structures of a thermophilic cyanobacterial light-harvesting phycobilisome. *Nat. Commun.* **2022**, 13, 3389.
15. Adir, N.; Lerner, N. The crystal structure of a novel unmethylated form of c-phycocyanin, a possible connector between cores and rods in phycobilisomes. *J. Biol. Chem.* **2003**, 278, 25926–25932.
16. Nganou, C.; David, L.; Adir, N.; Mkandawire, M. Linker Proteins Enable Ultrafast Excitation Energy Transfer in the Phycobilisome Antenna System of Thermosynechococcus vulcanus. *Photochem. Photobiol. Sci.* **2016**, 15, 31-44.
17. Hirota, Y.; Serikawa, H.; Kawakami, K.; Ueno, M.; Kamiya, N.; Kosumi, D. Ultrafast energy transfer dynamics of phycobilisome from Thermosynechococcus vulcanus, as revealed by ps fluorescence and fs pump-probe spectroscopies. *Photosynth. Res.* **2021**, 148, 181–190.
18. Kawakami, K.; Nagao, R.; Tahara, Y.O.; Hamaguchi, T.; Suzuki, T,; Dohmae, N.; Kosumi, D.; Shen, J.; Miyata, M.; Yonekura, K.; Kamiya, N. Structural implications for a phycobilisome complex from the thermophilic cyanobacterium Thermosynechococcus vulcanus. *Biochim. Biophys. Acta Bioener.* **2021**, 1862, 148458.
19. Adir, N.; Dines, M.; Klartag, M.; McGregor, A.; Melamed-Frank, M. Assembly and Disassembly of Phycobilisomes. In *Complex Intracellular Structures in Prokaryotes. Microbiology Monographs*, 1st ed.; Shively, J.M., Eds.; Springer Science & Business Media: Berlin/Heidelberg, Germany, **2006**; Volume 2, pp. 47 – 77.
20. Gantt, E.; Lipschul, C.A. Phycobilisomes of Porphyridium cruentum: I. Isolation. *J. Cell Biol.* **1972**, 54, 313-324.
21. Ducret, A.; Sidler, W.; Wehrli, E.; Frank, G.; Zuber, H. Isolation, Characterization and Electron Microscopy Analysis of A Hemidiscoidal Phycobilisome Type from the Cyanobacterium Anabaena, sp. PCC 7120. *Eur. J. Biochem.* **1996,** 236(3), 1010-1024.
22. Wang, H.; Zhao, J.; Jiang, L. Energy transfer processes in phycobilisome model complex at 77 K. *China Ser. B-Chem.* **2000**, 43, 233–239.
23. Zhao, F.; Zheng, X.; Zhang, J.; Wang, H.; Yu, Z.; Zhao, J.; Jiang, L. Energy transfer in allophycocyanin hexamer from Anabaena variabilis by time-resolved spectroscopy. *J. Photochem. Photobiol. B* **1998**, 45, 144–149.
24. Sandstrom, A.; Gillbro, T.; Sandstrom, U.; Fischer, R.; Scheer, H. Picosecond study of energy transfer within 18-S particles of AN112 (a mutant of Synechococcus 6301) phycobilisomes. *Biochim. Biophys. Acta Bioener.* **1988**, 933, 54–64.
25. Zhang, J.; Zhao, F.; Zheng, X.; Wang, H. Direct measurement of excitation transfer dynamics between two trimers in C-phycocyanin hexamer from cyanobacterium Anabaena variabilis. *Chem. Phys. Lett.* **1999**, 304, 357–364.
26. Xie, M.; Li, W.; Xiao, C.; Zhen, Z.; Ma, J.; Lin, H.; Qin, S.; Zhao, F. Time-Resolved Fluorescence Spectroscopy Study of Energy Transfer Dynamics in Phycobilisomes from Cyanobacteria Thermosynechococcus vulcanus NIES 2134 and Synechocystis sp. PCC 6803. *Crystals*, **2021**, 11, 1233.
27. Eisenberg, I.; Caycedo-Soler, F.; Harris, D.; Yochelis, S.; Huelga, S.F.; Plenio, M.B.; Adir, N.; Keren, N.; Paltiel, Y. Regulating the Energy Flow in a Cyanobacterial Light-Harvesting Antenna Complex. *J. Phys. Chem. B* **2017**, 121, 1240−1247.
28. Zhao, F.; Zhang, J.; Zheng, X.; Wang, H. Energy transfer among proteins in the phycobilisome of red algae. II. Energy transfer in synthesized complex of R-PE/R-PC and R-PE/APC. *Zhongshan Da Xue Xue Bao. Zi Ran Ke Xue Ban Acta Sci. Nat. Univ. Sunyatseni* **1998**, 37, 18–23.

 doi:10.20944/preprints202304.0938.v1